Geophys. J. Int. (2006) **164,** 301–311 doi: 10.1111/j.1365-246X.2005.02825.x

Beyond smooth inversion: the use of nullspace projection for the exploration of non-uniqueness in MT

G. Muñoz[1] and V. Rath[2]

[1]*Departament de Geodinamica i Geofisica C/Marti i Franques s/n, Universitat de Barcelona,* E-08028, *Barcelona. E-mail: gmunoz@geo.ub.es*
[2]*Applied Geophysics, RWTH Aachen University, Lochnerstr.,* 4-20, D-52056 *Aachen, Germany*

Accepted 2005 October 4. Received 2005 August 6; in original form 2004 November 25

SUMMARY

Regularized inversion is the most commonly used interpretation method for magnetotellurics (MT) data. This leads to smooth models, which minimize the differences between the model response and the observed data. These models, however, do not represent the only possible solution. The inherent non-uniqueness of the problem and the errors in the data lead to the existence of equivalent models, that is, different models with very similar responses.

Traditionally, equivalent models have been studied by using the singular value decomposition (SVD) of the Jacobian matrix (also known as the sensitivity matrix). The sensitivity matrix relates small changes in the model parameters with the associated changes in the response. By adding a linear combination of singular vectors of the nullspace of the sensitivity matrix to a model vector (in the parameter space), the resulting model has the same fit to the data as the original model. This approach has been used successfully to construct equivalent models in 1-D cases, represented by a small number of parameters. The application of this technique to 2-D or 3-D cases, however, is unpractical because of the large number of parameters involved. This makes the intuitive interpretation of the singular vectors in physical and geological terms impossible.

In this paper, we present a hybrid algorithm, which seeks to unite the desirable features of the probabilistic and deterministic approaches to model appraisal; it generates a collection of models by a random modification of the segmented geoelectrical image's geometry. This represents a limited exploration of a subset of the parameter space characterized by similar geometry. We can then efficiently construct conservative models by projecting the changes introduced by the modification algorithm onto the nullspace of the original problem, thus maintaining the obtained fit to the data (in the linear approximation). In this way it is possible to test the structures obtained in 2-D MT inversions with respect to their resolution and inherent equivalencies. To illustrate the method, several numerical experiments with different structures and conditions are presented. In addition to these synthetic examples, a case study from SW Iberia is also shown.

Key words: inverse theory, magnetotellurics, numerical techniques, sensitivity.

1 INTRODUCTION

In electromagnetic methods, and magnetotellurics (MT) in particular, the problem of equivalency is well known; there are different models with response differences smaller than the data errors.

Measured data are usually interpreted by seeking a model, which explains them in a given way. Some type of least-squares method is commonly applied for this purpose, minimizing the squared differences between the model response and the observed data. In geophysical inversion, however, this procedure does not always lead to a satisfactory model, such problems being ill-posed due to the inherent physical non-uniqueness, erroneous assumptions in the modelling, and the presence of errors in the data and model. All of these often cause an instability of the solution. While all of the mentioned shortcomings may contribute to the ill-posedness of the inverse problem, the problem of instability can be remedied by using a regularization functional that incorporates additional constraints on the solution (Tikhonov & Arsenin 1979) and takes into account prior information (Tarantola & Valette 1982a,b; Tarantola 2004). One of the most successful methods of this type is based on minimizing model roughness (e.g. de Groot-Hedlin & Constable 1990; Rodi & Mackie 2001). Models resulting from this approach are smoothed images of the true geoelectrical structures. This approach is by no means the only possibility, and other regularization functionals may be used, such

as focusing operators (Portniaguine 1999; Portniaguine & Zhdanov 1999) introduced to MT lately (Zhdanov 2002; Mehanee & Zhdanov 2002). Clearly, none of these approaches is inherently superior to the others, as none guarantees that the resulting model is physically acceptable or near to the true structure of the subsurfaces.

Although smooth inversion usually leads to stable models, there are many problems associated with this approach. Firstly, nature is not always smooth: faults and other discontinuous tectonic elements are not well represented by a smooth geoelectric image. Regularization by smoothing favours extended bodies of moderate conductivity instead of well-localized sharp conductivity contrasts. Thus, there is no guarantee that the obtained model is physically and geologically reasonable. The classical solution to this problem is the continued application of forward modelling in order to test whether a given geological conception is consistent with the data. While usually giving satisfactory results, this approach can be quite time consuming, and is of course biased by the researcher's preconceptions. Alternatively, the model space can be explored by an exhaustive probabilistic method (Mosegaard & Tarantola 2002; Mosegaard & Sambridge 2002), often requiring extensive computer resources. It would thus be extremely useful for researchers to have a method that combines the objective character of the probabilistic simulation with the incorporation of prior knowledge.

We present a new technique that allows the geometry of bodies to be changed at random while using information from the deterministic inversion in order to maintain the fit to data (i.e. it generates equivalent models in the linear approximation) and which avoids the manual edition of the models. Model appraisal is based on a nullspace projection technique to obtain conservative models from a collection of model modifications. In this way it is possible to test the structures obtained in 2-D MT inversions with respect to their resolution and inherent equivalencies. The nullspace projection technique was first used by Deal & Nolet (1996), and subsequently by Rowbotham & Pratt (1997), to improve the seismic tomographic inversion. As the technique avoids continued forward modelling, the computational time is reduced considerably because the projector is calculated only once and can be used for the different models rather than calculating the response for each one. Though some of the examples in this study have been taken from the results of a smooth inversion scheme (Mackie *et al.* 1997; Rodi & Mackie 2001), it must be emphasized that the approach does not depend on the specific inversion scheme employed, but may be used with all of the mentioned schemes, as long as appropriate sensitivity matrices are available.

In this paper we will first introduce the concepts on which this method is based, and then present several case studies which illustrate its application to synthetic and field data.

2 PREVIOUS WORK

Regularized inversion begins with a functional that defines the sense in which the model explains the data. In least-squares theory the fit of the data is defined by squared residuals. As pointed out above, this does not usually lead to a unique solution and thus some kind of regularization is required. In particular, the 2-D inversion algorithms most commonly employed in MT (e.g. Mackie *et al.* 1997; Rodi & Mackie 2001; Siripunvaraporn & Egbert 2000) use the following objective function, which is minimized by an iterative scheme:

$$\theta = \|\mathbf{w}_d(\mathbf{d} - \mathbf{g}(\mathbf{m}))\|_2^2 + \tau \left\|\mathbf{w}_m(\mathbf{m} - \mathbf{m}_{apr})\right\|_2^2. \quad (1)$$

Here the first term represents the weighted Euclidean norm of the residuals (difference between the data and the model response). The weighting matrix $\mathbf{w}_d$ is usually assumed to be diagonal with the inverses of the data variances as its elements. The second term defines the nearness of the model to an *a priori* model. In this case the weighting matrix $\mathbf{w}_m$ is not diagonal but rather a discrete roughening operator like the first or second spatial derivative of the parameters. The multiplicative term τ is a trade-off parameter that has to be determined. It represents the relative importance given to the data fit and model norm. There are many possibilities determination of τ. Among the most popular are (1) the use of the discrepancy principle, (2) the L-curve method or (3) generalized cross-validation, which all are described by Hansen (1998). They have recently been tested in electromagnetic inverse problems by Farquharson & Oldenburg (2004). Most researchers prefer simpler heuristic methods, however, because the aforementioned methods require the knowledge of error structure as (1), or the solution of many forward problems (2, 3), rendering the method computationally expensive. There are possible remedies for this, for example, the transformation of the linear equations to shifted systems, which can be solved very effectively for many τ (van den Eshof & Sleijpen 2004; Frommer & Maass 1999). Among the heuristic methods for choosing τ there are cooling schedules (e.g. Newman & Hoversten 2000), starting with large a τ, reducing it until the solution shows indications of instability. One then chooses a value of the regularization parameter just above this value. As in any regularization scheme of the type described in this study, this represents a trade-off between data fit and model regularity. For the field examples presented later, after an initial stage of experimental inversions with the code of our choice (Mackie *et al.* 1997), it was decided to use first-difference regularization (i.e. enforcing the 'flattest' model), and the regularization parameter τ was fixed for all subsequent runs.

Functional (1) can be minimized by standard Gauss–Newton techniques based on differentiating the non-linear forward operator $\mathbf{g}$ with respect to the parameters $\mathbf{m}$ in order to obtain the Jacobian matrix, $\mathbf{J}$ (sometimes called the sensitivity matrix). It is an $N \times M$ matrix (where N is the number of data and M is the number of parameters) that maps the parameter space onto the data space. The parameter semi-norm is easily differentiated because of its inherent linear character. We obtain an equation system, which is solved using an appropriate method and the solution to the original non-linear minimization problem is found by a series of linear steps. As the calculation of $\mathbf{J}$ is generally the most time-consuming part of inversion algorithms it is often avoided in advanced codes by using a variant of non-linear conjugate gradient algorithms or quasi-Newton methods (Nocedal & Wright 1999). Here only the product of $\mathbf{J}$ or its transpose, $\mathbf{J}^T$, with some vectors is necessary. We will argue in this paper, however, that this matrix, once obtained, carries a large amount of information about the internal structure of the problem, and can be used for the estimation of errors and further methods of model appraisal.

Sensitivity studies based on columnwise sums of the sensitivity matrix have been used to indicate, which model parameters are less resolved by the data and, therefore, should not be included in the interpretation (Schwalenberg 2000; Schwalenberg *et al.* 2002). Traditionally, equivalent models have been studied (e.g. Pous *et al.* 1985) by using the singular value decomposition (SVD) of the sensitivity matrix. By adding a linear combination of singular vectors associated with zero-valued (or very small) singular values of the sensitivity matrix to the model vector (in the parameter space), the resulting model presents the same fit to data as the initial model. This technique proves useful with simple models and has only been implemented in 1-D models (e.g. Pous *et al.* 1985; Pedersen &

Rasmussen 1989), which can be represented by a reduced number of parameters and have a sensitivity matrix that can be computed analytically. The singular vectors in simple cases have a very intuitive meaning and most of the equivalencies show up as linear combinations of logarithmic parameters.

2-D or 3-D models are characterized by finite element or finite difference meshes, which are constructed from a large number of cells (in the range of a few hundred to a few thousand for 2-D and even higher for 3-D). In these cases such a large number of cells is necessary to obtain accurate results for the forward problem. To reduce the degrees of freedom, we can fix the geometry of distinct bodies with associated unique conductivities, but this is undesirable because our conception of the geometry may be wrong. That leaves us with the original cell conductivities as inversion parameters. At least in 2-D cases, the sensitivity matrix is computed numerically in most inversion algorithms and its SVD can be efficiently performed by optimized standard software (e.g. LAPACK, Anderson *et al.* 1999), although the intuitive interpretation of the singular vectors is no longer possible. Furthermore, unlike in some simple 1-D models, the singular values often do not show clear discontinuities suggesting a cut-off value for SVD truncation. This can be seen in Fig. 1.

Given appropriate assumptions regarding errors in the observed data, estimates of parameter errors can be derived with the help of the sensitivity matrix (Tarantola & Valette 1982a; Menke 1984). Although knowing error bars is very helpful in the assessment of model quality, the calculation of these quantities is rather cumbersome due to the large and densely populated matrices involved. This is equally true for the usual measures of resolution such as the resolution matrix or the information density matrix. As an example, Fig. 2 displays the diagonal of the resolution matrix for two synthetic models (described in detail later). In these cases the resolution matrix clearly highlights the areas which are well resolved.

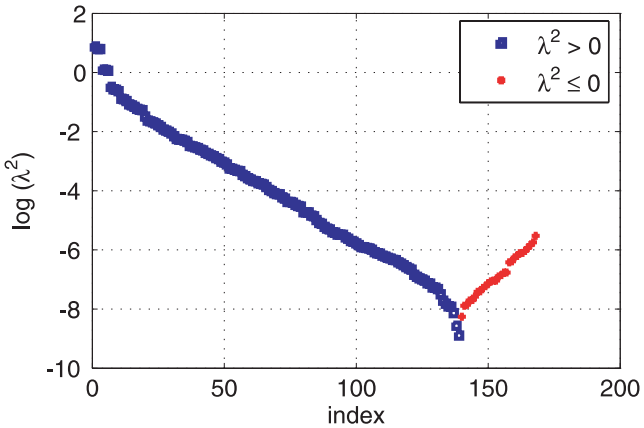

Figure 1. Singular value spectrum for a simple model consisting of a block of 10 Ωm above another block of 1 Ωm in a 100 Ωm half-space. The smallest singular values are strongly affected by numerical errors and can even become negative (red, plotted in positive direction).

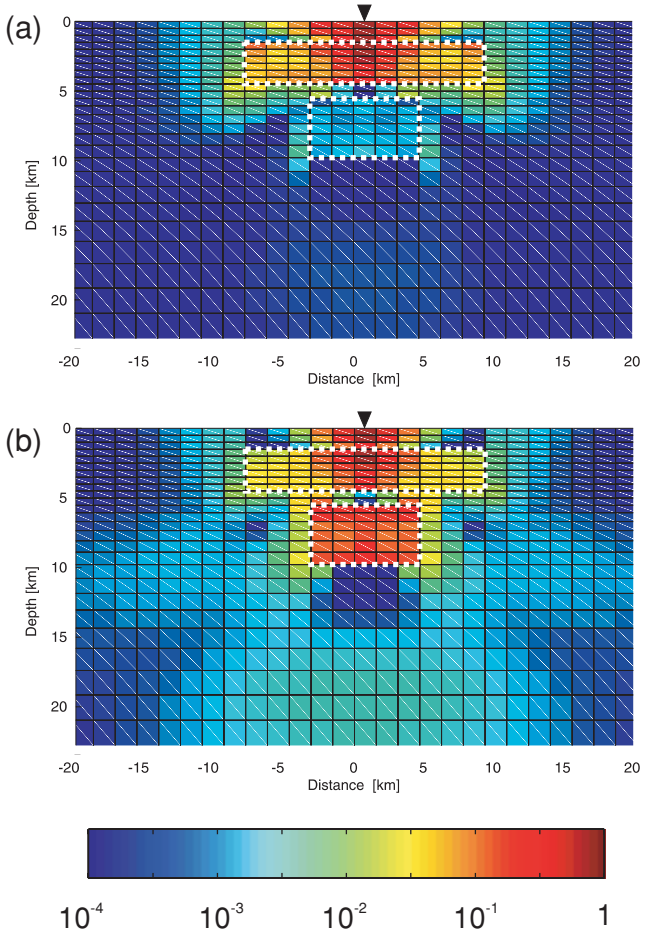

Figure 2. Representation in grid form of the main diagonal of the resolution matrix for two simple models consisting of two blocks (1 and 10 Ωm) in a 100 Ωm. In Fig. 2(a) the 1 Ωm block is above the 10 Ωm one and in Fig. 2(b) their positions are reversed.

3 OUTLINE OF THE METHOD

The algorithm presented here consists of two distinct building blocks: a first component that generates modified models from a starting one (either obtained from inversion or a synthetic test model) and a second component in which the differences between the trial model and the original model are projected onto the nullspace, enabling the resulting model to be found. The use of the random modification algorithm provides a collection of models so that different features of the resistivity structures can be appraised. This is different from a probabilistic approach in the sense that only a predefined subset of the parameter space is considered. On the other hand, the second component(i.e. the projection onto the nullspace) can be used independently using a preferred trial model in order to check the compatibility of some particular features with the data.

3.1 Model modification

The model modification algorithm (schematically presented as a flow chart in Fig. 3) generates a series of models by randomly modifying the geometry of a specified area of the starting model. As inputs we use the starting model, stating the area to be modified and a set of resistivities that will be used in the generation of the random models. The last resistivity of the set is taken as the background resistivity, and the others as anomalous resistivities. The algorithm uses the following scheme:

(i) The specified area of the starting model is segmented using the previously stated resistivity levels.

(ii) For each of the anomalous resistivities (indexed starting from the innermost) the area occupied by resistivities with indices equal

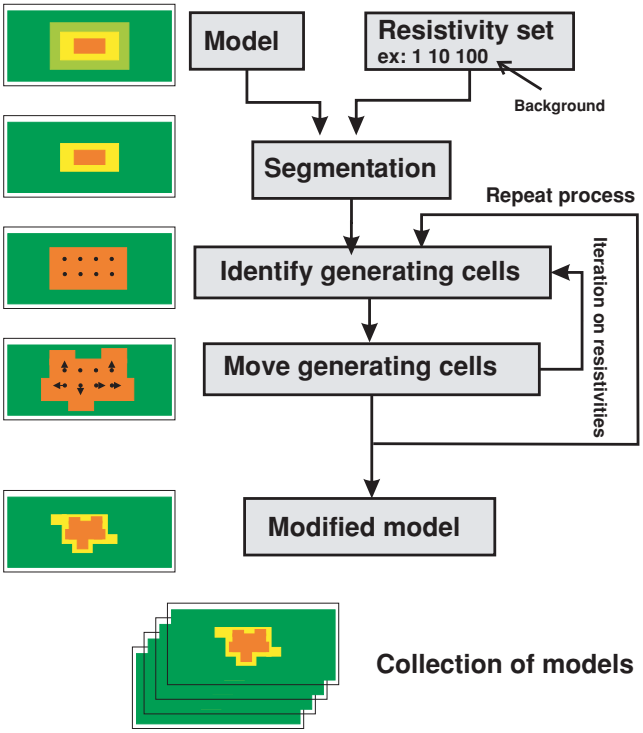

Figure 3. Flow chart for the model modification scheme. See text for explanations.

or lower than the considered resistivity is identified. This area is the basis for the definition of the 'generating cells'. We call 'generating cells' those which are completely surrounded by other cells belonging to this area. Thus, we consider each of the bodies made up of overlapping blocks of 3 × 3 cells each. Overlapping blocks are used to prevent the bodies from being disintegrated. Note that if a feature smaller than a 3 × 3 block exists, it will not be taken into account by the algorithm, and so will be lost.

(iii) The position of the generating cells of each anomalous resistivity is displaced in a randomly chosen direction (up, down, left, right, or remain in the same position) according to a given probability for each direction. In this way we can bias the modification process, for example, to produce elongated vertical structures like faults.

(iv) The model is rebuilt by placing a 3 × 3 block centred on each of the generating cells.

(v) The whole process is repeated for a given number of iterations. Note that, at each iteration, the modified model presents greater differences compared with the starting model.

Fig. 4 demonstrates the generating cells approach, and gives a sample set of modifications applied to a simple starting model. In these examples, only two resistivities are used: a background of 100 Ωm and an anomaly of 10 Ωm. As can be seen, there is a trend towards increased anomaly size at each iteration. We observed this to be a typical behaviour in all the tests performed, and believe the effect is due to the random nature of the modification process. As we are usually interested in minimal structures, a size control feature can be enabled in order to avoid this effect. This feature counts the number of cells of the anomaly before and after every iteration. If the size has increased more than a pre-set amount, the iteration is rejected and the process is repeated from the last accepted iteration. Using a value less than 1, a shrinking of the body can be enforced.

From this point, a model from the generated collection could be used in forward modelling, checking whether it fits the data well enough. This would be the more general approach, one not dependent on any linearization. As explained before, however, forward modelling can be rather time consuming and so a faster alternative was sought.

3.2 Nullspace projection

The nullspace projection algorithm applied here was originally used by Deal & Nolet (1996) and later by Rowbotham & Pratt (1997) to improve the results of seismic tomography. This approach is based on the SVD of the sensitivity matrix and is used to determine the permissible changes caused by small modifications of the model such that the data fit is conserved.

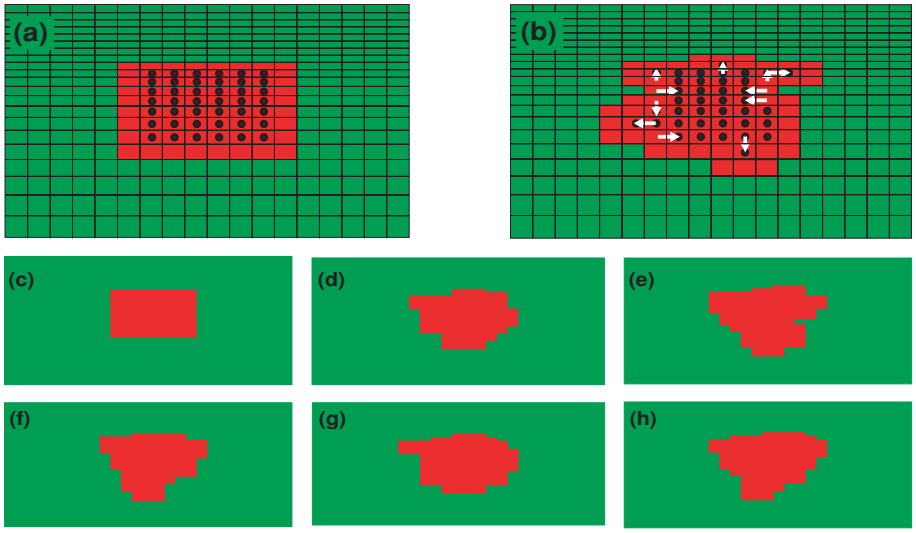

Figure 4. Example illustrating the generating cells approach for the model modification scheme. (a) shows the generating cells for a single block model with only one level of anomalous resistivity present. (b) shows the effect of one deformation cycle and the new positions of the generating cells. (c)–(h) is a sequence of deformation.

The linearized forward problem is expressed as

$$\mathbf{d}(\mathbf{m}) = \mathbf{d}(\mathbf{m}_0) + \mathbf{J} \cdot (\mathbf{m} - \mathbf{m}_0), \tag{2}$$

or

$$\Delta\mathbf{d} = \mathbf{J}\Delta\mathbf{m}, \tag{3}$$

where $\mathbf{d}$ is an N-dimensional vector containing the data and $\mathbf{m}$ is an M-dimensional vector containing the model parameters. The matrix $\mathbf{J}$ is known as the sensitivity matrix and its elements are the partial derivatives of the data with respect to the model parameters. The higher-order terms are neglected for the linear approximation.

The SVD for a matrix was introduced by Lanczos (1961) and, for $\mathbf{J}$, it can be expressed as

$$\mathbf{J} = \mathbf{U}\mathbf{\Lambda}\mathbf{V}^T. \tag{4}$$

The matrix $\mathbf{U}$ is a matrix of singular vectors that span the data space, $\mathbf{V}$ is a matrix of singular vectors that span the parameter space, and $\mathbf{\Lambda}$ is a matrix whose diagonal elements are the singular values of the sensitivity matrix. The matrices in the previous equation can be partitioned into range (non-zero singular values) and nullspace (zero-valued singular values), so that

$$\mathbf{J} = \mathbf{U}_p\mathbf{\Lambda}_p\mathbf{U}_p^T, \tag{5}$$

where p denotes that the SVD has been truncated and only the p non-zero singular values have been retained. The rejected columns of $\mathbf{V}$ span the nullspace of $\mathbf{J}$. The matrix $\mathbf{V}_{\text{null}}$ is defined as the matrix of those columns of $\mathbf{V}$ excluded from $\mathbf{V}_p$. With actual sensitivity matrices, the partition between non-zero and zero singular values is not obvious, and a threshold has to be established in order to decide which values are considered zero (and thus part of the numerical nullspace) or non-zero (and part of the numerical range). The nullspace thus obtained depends on this partitioning, and choosing the threshold is crucial for the success of the method. The implications of an incorrect selection will be discussed later.

The SVD of the sensitivity matrix $\mathbf{J}$ can be performed by computing the eigenvalues and eigenvectors of either the matrix $\mathbf{J}\mathbf{J}^T$ or the matrix $\mathbf{J}^T\mathbf{J}$. In both cases, the p non-zero singular values λ are the same. In the former case, the corresponding eigenvectors generate the matrix $\mathbf{U}$, and thus span the N-dimensional data space. The vectors of $\mathbf{V}_p$ can be calculated from the vectors of $\mathbf{U}_p$, the matrix $\mathbf{J}$ and the corresponding eigenvalues. In the latter case, the associated singular vectors generate the matrix $\mathbf{V}$, spanning the M-dimensional parameter space. In an analogous way, the matrix $\mathbf{U}_p$ can be calculated from $\mathbf{V}_p$, $\mathbf{J}^T$ and the singular values. In most 2-D MT models the dimension of the parameter space (the number of cells in the mesh) is higher than the dimension of the data space ($M \gg N$) and, therefore, the computation time can be reduced by performing the SVD using the matrix $\mathbf{J}\mathbf{J}^T$.

Assuming that the linear approximation is justified, we construct a model change vector ($\Delta\mathbf{m}$) as a linear combination of vectors of the nullspace. The resulting change in the data space is

$$\Delta\mathbf{d} = \mathbf{J}\Delta\mathbf{m}_{\text{null}} = \mathbf{U}_p\mathbf{\Lambda}_p\mathbf{V}_p^T \cdot \Delta\mathbf{m}_{\text{null}}. \tag{6}$$

The vector $\Delta\mathbf{m}_{\text{null}}$ is a linear combination of vectors of $\mathbf{V}_{\text{null}}$, which is orthogonal to $\mathbf{V}_p$, so the product $\mathbf{V}_p^T\,\Delta\mathbf{m}_{\text{null}}$ is zero and, therefore, $\Delta\mathbf{d} = 0$. So, the data fit for $\mathbf{m}_c = \mathbf{m}_0 + \Delta\mathbf{m}_{\text{null}}$ is expected to be the same as $\mathbf{m}_0$, and thus $\mathbf{m}_c$ and $\mathbf{m}_0$ are equivalent models (and $\mathbf{m}_c$ may be called a conservative model). As discussed before, in 2-D MT, models are characterized by several thousands of parameters and constructing a linear combination of vectors of $\mathbf{V}_{\text{null}}$ based on physical and geological considerations is not obvious. The nullspace shuttle approach consists in using a geometrical deformation of the starting model (for instance, the modified model obtained in the previous section or a test model) and then projecting the differences onto the nullspace. Therefore, the projected vector change is guaranteed to be a linear combination of nullspace vectors while being close to the geometrical deformations introduced by the first step.

The projection matrix or projector is computed from the range of $\mathbf{V}$, namely

$$\mathbf{P} = \mathbf{I} - \mathbf{V}_p\mathbf{V}_p^T = \mathbf{V}_{\text{null}}\mathbf{V}_{\text{null}}^T, \tag{7}$$

where $\mathbf{I}$ denotes the $M \times M$ identity matrix.

Taking into account the expression for the resolution matrix $\mathbf{R} = \mathbf{V}_p\mathbf{V}_p^T$ (Menke 1984), it can be easily seen that both matrices are closely related. Without truncation, that is, $p = M$, the resolution matrix becomes the identity and thus the projector vanishes. In this case there will not be equivalent models as any model modification will be projected onto the original model (see eq. 8 below). Although both forms given in eq. (7) can be used to calculate the projector, the first one is preferred because generally the number of small singular values is large. Furthermore, small eigenvalues are more prone to numerical error and small-scale features in the model.

A conservative model is then constructed by adding the projected model change to the starting model:

$$\mathbf{m}_c = \mathbf{m}_0 + \mathbf{P} \cdot \Delta\mathbf{m}. \tag{8}$$

Note that the projector is unique to each starting model. Once calculated and stored we can generate a large collection of equivalent models $\mathbf{m}_c$ by using eq. (8) with different $\Delta\mathbf{m}$.

3.3 Choosing the threshold

One problem with the SVD decomposition is the truncation of the matrix $\mathbf{V}$. In practice, the singular values are not divided simply into non-zero and zero values.

The matrix $\mathbf{V}_p$ is computed from the singular vectors with singular values that satisfy

$$\lambda > \varepsilon\lambda_{\max}, \tag{9}$$

where $\lambda_{\max}$ is the biggest singular value and ε is a threshold that can be defined. The value of ε is usually estimated from a plot of the eigenvalue spectrum. As can be seen in Fig. 1, the eigenvalue spectrum does not display a clear discontinuity but rather a continuous descent. This makes it quite difficult to decide on the value of ε in a plausible way.

When in doubt as to whether a singular value should be considered part of the range or the nullspace, we propose using a conservative criterion in choosing the smallest possible value for the threshold ε. If an eigenvalue that should be considered null is not included, we are losing some of the equivalencies, but if non-zero eigenvalues are used to compute the numerical nullspace, the fit to the data will no longer be maintained. The effect of choosing different values for ε is illustrated in Fig. 5. Note that forward modelling can be used to check whether the chosen truncation threshold leads to a really equivalent model or shows signs of contamination. This approach can, of course, be rather slow but sometimes it is the only way to properly determine the truncation threshold.

4 SYNTHETIC EXAMPLES

To illustrate the method, we present several numerical experiments with different structures and conditions. All the sensitivities for these synthetic models were calculated using the code of (Mackie

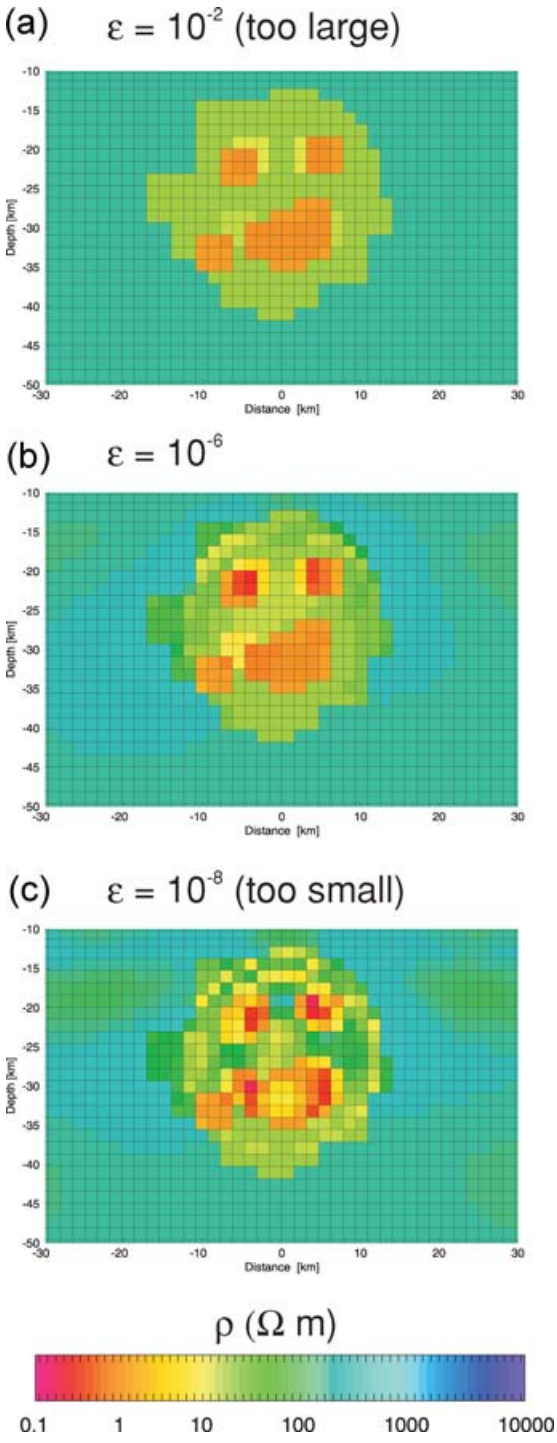

Figure 5. Example illustrating the effect of choosing different truncation thresholds. These models are obtained by applying the modification scheme and the subsequent projection to a model constructed from a large 10 Ωm conductor embedded in a 100 Ωm background, with several small-scale anomalies of 1 Ωm inside (see Section 4 for further details on this). Panel (a) shows a conservative model constructed with $\varepsilon = 10^{-2}$, which is definitely too high. In this case the conservative model closely resembles the modified model (note that the 'conservative' model does not maintain the fit to data). In Fig. 5(c) the conservative model was constructed with $\varepsilon = 10^{-8}$, a too small value. In this case, the projector is dominated by eigenvectors associated with negative eigenvalues (see Fig. 1, red) which are strongly affected by numerical errors. Fig. 5(b) shows a conservative model constructed with an appropriate value for the threshold ($\varepsilon = 10^{-6}$).

et al. 1997). Note that this version of the code does not include the geomagnetic transfer functions and so these could not be taken into account.

The first example consists of a 100 Ωm half-space with a shallow conductive anomaly of 10 Ωm and a deep conductive anomaly of 1 Ωm (Fig. 6a). In this case we do not use the model modification algorithm proposed in this paper, but a trial model consisting of the same starting model but without the deep conductive body (Fig. 6b). The data consist of apparent resistivity and phases for both TE and TM modes at 14 frequencies ranging from 32 Hz to 100 000 s at three sites. The SVD truncation threshold was set to $\varepsilon = 10^{-6}$. The result of the projection is shown in Fig. 6(c). The conservative model is exactly the same as the starting model, so we can say that the deep conductive anomaly is really required by the data.

The second example is a model very similar to the previous one, but with the resistivities of the anomalies reversed. The shallow anomaly now has a resistivity of 1 Ωm, while the deep one has a resistivity of 10 Ωm (Fig. 6d). The trial model approach is used again, using the model without the deep anomaly (Fig. 6e). The data consist of the same sites and frequencies as in the previous model, and the value of ε is also 10^{-6}. Fig. 6(f) shows the conservative projected model. It can be seen that the deep conductor is no longer present in the equivalent model. Therefore, it is not necessary to explain the data. This effect is well known, as the upper conductive body screens the features below and they are not detectable.

These two, very simple examples serve to show how the algorithm is capable of reproducing positive and negative results. In the first case, we have an example of a positive result, that is, the anomaly is required by the data and thus is recovered from the projection, even though it was completely removed in the test model. In contrast, the second case is an example of a negative result; the data are not sensitive to the resistivity of the deep anomaly and thus it can be removed without altering the fit to data (as shown in the projection). These results are not surprising as they could be observed in the resolution matrices presented in Fig. 2 (containing the same information as the projector).

The third synthetic example is more complex. We start with the model in Fig. 7(a). There is a background of 100 Ωm and a large 10 Ωm anomaly with small-scale details of 1 Ωm inside (a smiley). The data consist of apparent resistivity and phases for both TE and TM modes at 5 sites and 13 frequencies ranging from 10 Hz to 10^6 s. We apply the model deformation algorithm to generate geometrical variations in the model. Figs 7(b) and (d) show the effect of three and five iterations of the algorithm, respectively. In order to generate these models the size control feature was enabled and the probability of upwards displacement was doubled with respect to all other directions. In this way, we can simulate a reduction in the depth of the bottom of the structures.

By comparing these images with Figs 7(c) and (e) we can gain some insight into the sensitivity of data to the different structures. In Fig. 7(b), it can be seen that the modified model presents a shallower bottom than the starting model, and that the 'eyes' have been merged. The respective projection (Fig. 7d) shows that the true position of the eyes is recovered, thus indicating that the data can resolve these small structures. However, the depth of the bottom is left as it is in the deformed model, so we can say that the data cannot resolve the depth of the bottom of the structure. The shape of the 'smile' is also deformed in the projected model; its geometry is not well resolved by the data. Fig. 7(d) shows, in addition to the effects already described, a lateral variation on the right side of the anomaly. In the projected model of Fig. 7(e) the true position of the conductive

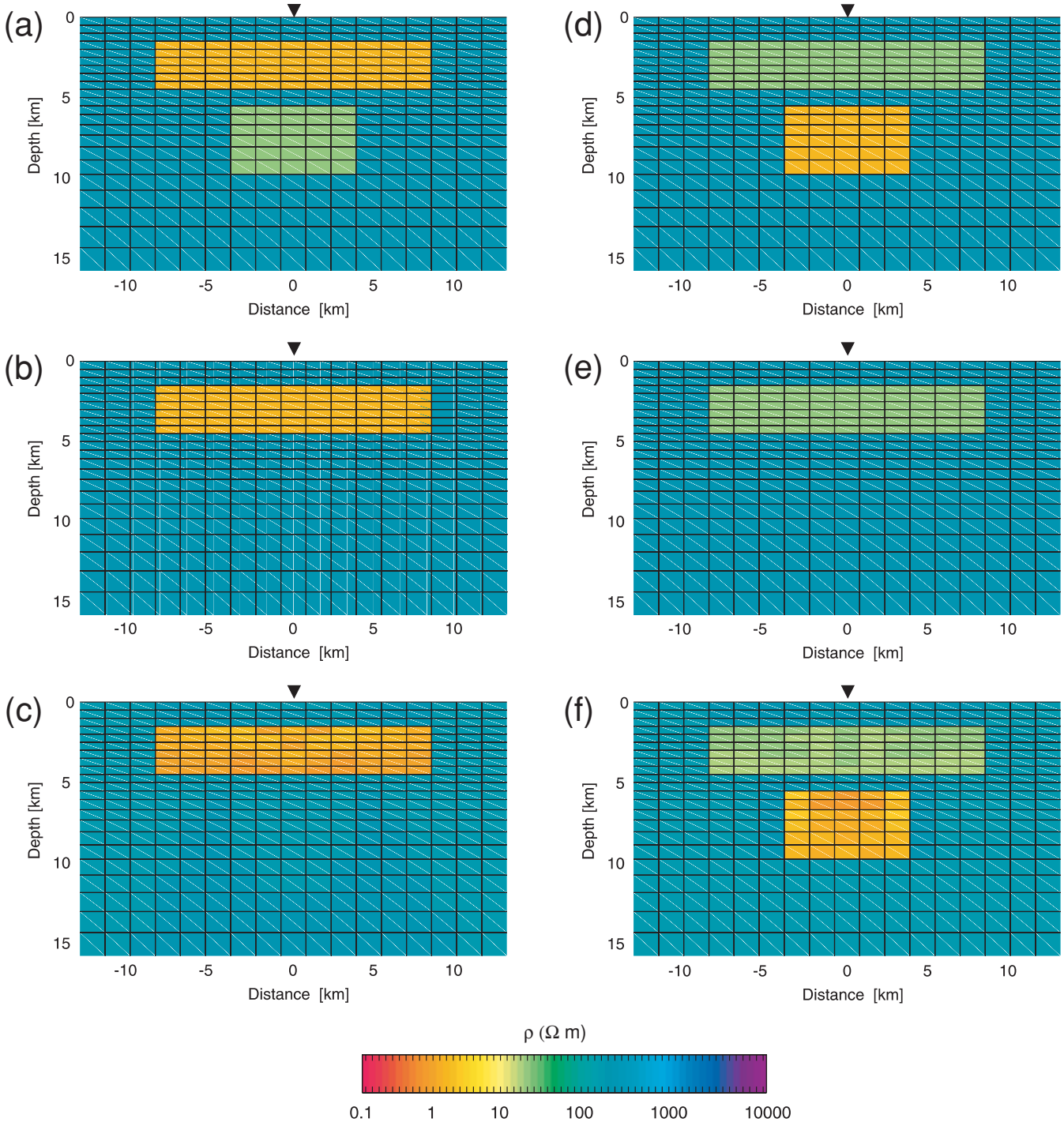

Figure 6. Original (a), modified (b) and projected (c) models for a simple two-block structure (10 Ωm anomaly over a 1 Ωm anomaly). Note that the deepest conductor is really required by the data and thus is recovered by the projection. Original (d), modified (e) and projected (f) models for a simple two-block structure (1 Ωm anomaly over a 10 Ωm anomaly). Note that, as illustrated by the projection, the deepest conductor is not required by the data.

body is recovered, indicating that the data are capable of resolving the horizontal position of the anomaly.

5 A CASE STUDY FROM SW IBERIA

The Iberian Massif is one of the best exposed fragments of the Variscan orogen in Europe. The Southern Branch was built up by the collision of three continental terranes: the South Portuguese Zone (SPZ), the Ossa Morena Zone (OMZ) and the Central Iberian Zone (CIZ). These blocks are separated by suture zones: the Pulo do Lobo Unit and the Beja-Acebuches ophiolitic complex between the SPZ and the OMZ; and the Central Unit between the OMZ and the CIZ. This area has been the subject of several MT surveys (Monteiro Santos *et al.* 1999, 2002; Pous *et al.* 2004) and structures of high conductivity related to the suture zones have been found.

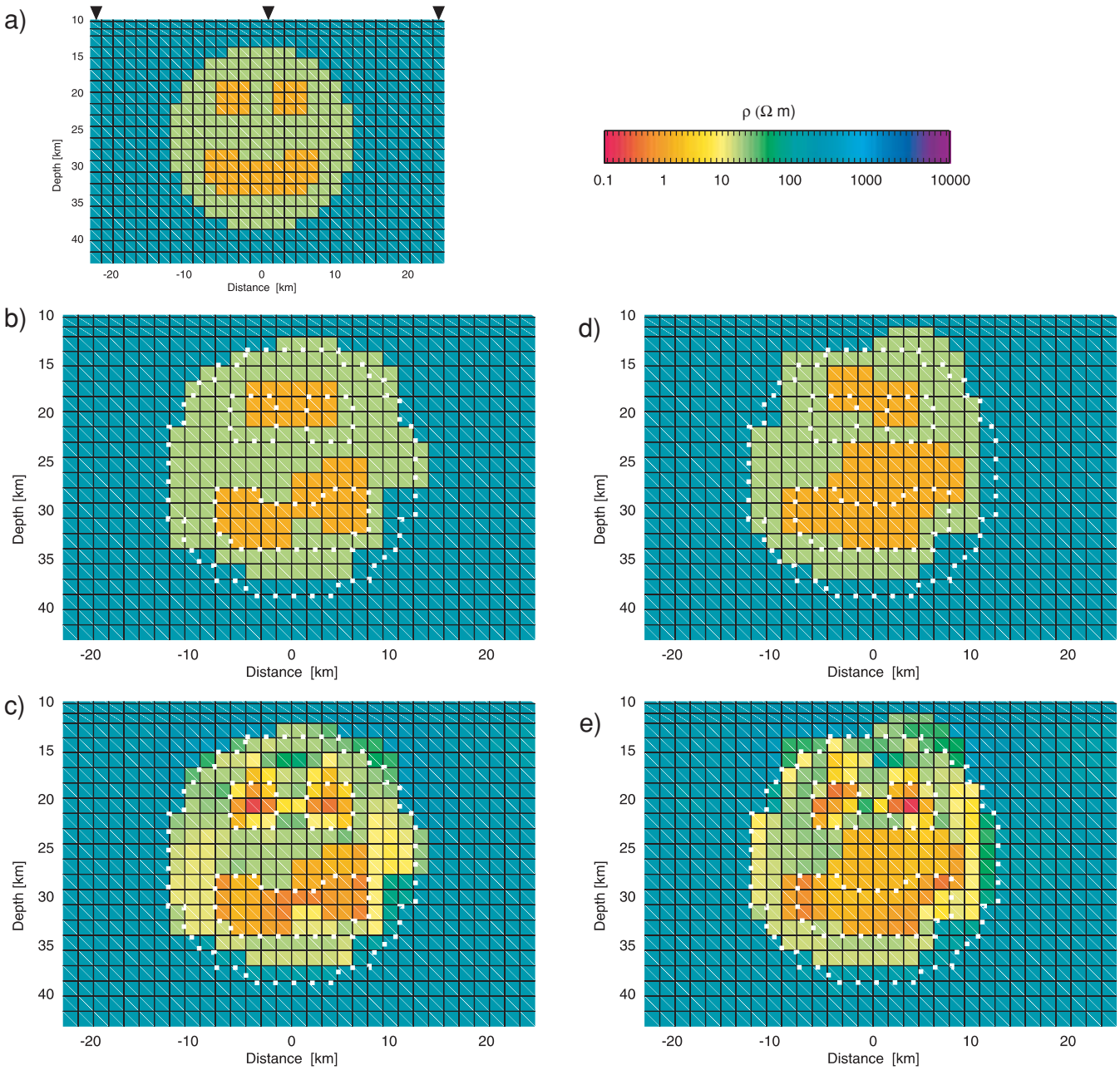

Figure 7. Example of the nullspace projection algorithm applied to a synthetic model. See text for details.

The authors relate the origin of the high conductivity to the presence of graphite-bearing rocks in the suture zones.

For our experiments we refer to the easternmost MT profile reported in Pous *et al.* (2004). Based on the dimensionality analysis, the authors divide the profile into two parts: one comprising the SPZ, the southern suture and part of the OMZ, with a strike angle of N125E; and another one along the whole OMZ, the Central Unit and the CIZ, with a strike of N105E. A sensitivity study using the nullspace projection algorithm was performed on the southern part of the profile (Fig. 8). A shallow conductor (not seen in the figure) correlates with the Iberian Pyrite Belt, another conductor is associated with the Pulo do Lobo accretionary prism and the big conductive body C is related to the main suture (Fig. 8a). As we are interested in determining the depth of the suture the area of study is centred on the conductor C. The data consist of apparent resistivity and phases for both TE and TM modes at 14 sites (marked on the figure are the sites from 5 to 11) and 38 periods ranging from 0.006 to 4000 s. After plotting and examining the singular value spectrum the truncation threshold for the matrix $\mathbf{V}_p$ was established at $\varepsilon = 10^{-6}$.

In this example, instead of working with the model modification algorithm, we adopted the trial model approach in order to gain some insight into the limits of the technique. Several test models were used reducing drastically the size of the conductor C, and even removing it completely. In all cases, the nullspace projection recovered the position and approximate geometry of the conductor in the starting model. Fig. 8(b) shows one of the test models with a reduced depth to bottom in the conductor under study. The equivalent model

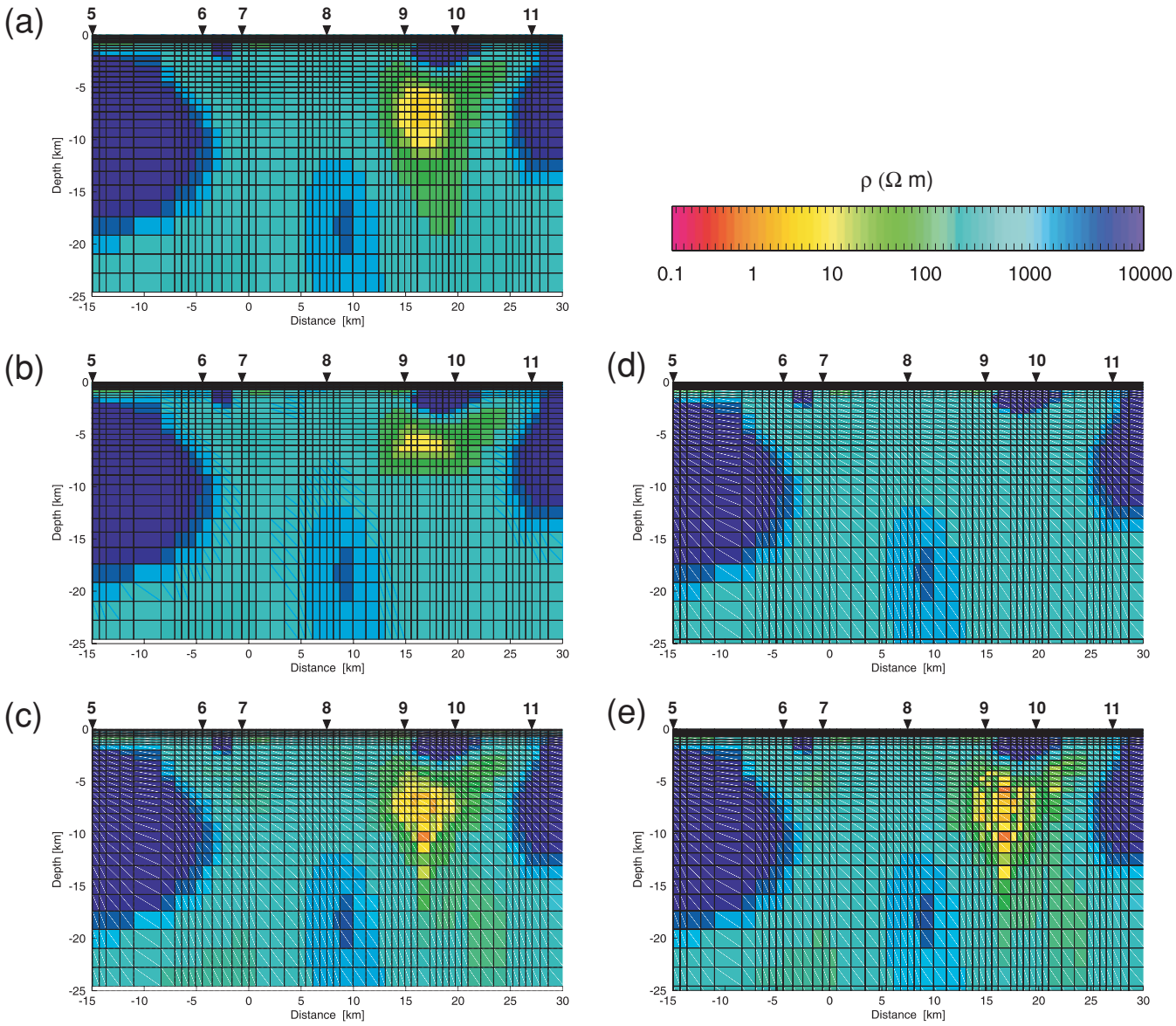

Figure 8. Application of the nullspace projection to a model from SW Iberia. To investigate the possible depth extent of anomaly obtained from inversion (a) its depth was reduced (b) and the whole conductor was completely removed (d). The projection recovers an anomalous body in both cases (c and e).

shown in Fig. 8(c) points to a slightly smaller conductor than in the starting model, with a bottom depth of only 15 km and a reduced width. Fig. 8(d) shows the model with the conductor C completely removed. Its associated projection, shown in Fig. 8(e), reintroduces the conductive feature. Note that the geometry of the upper part of the conductive body is stable in both projected models. The conductor in Fig. 8(e) is again smaller than the original and shows a 'noisy' appearance. The latter is, of course, due to the lack of regularization as only the Jacobian is used for the construction of the projector. Of course, it would be possible to construct a projector using the Jacobian augmented with a regularizing term. The result of this procedure is arguable, however, because the nullspace of this new operator should be 'small', if the regularization acts correctly.

Therefore, we can be sure that a high conductivity region exists in the area of the suture extending to a depth of at least 15 km. Its width, however, is not required to be as large as the smooth inversion suggests.

6 CONCLUSIONS

We have presented a hybrid algorithm, which seeks to unite the desirable features of both the probabilistic and deterministic approaches to model appraisal; it generates a collection of models through a random modification of the segmented geoelectrical image's geometry. This represents a limited exploration of a subset of the parameter space characterized by similar geometry. We can then efficiently construct conservative models by projecting the changes introduced by the modification algorithm onto the nullspace of the original problem, thus maintaining the obtained fit to the data. Though constructing projected models is much faster than forward modelling, the calculation of the SVD may be a demanding task, in particular when 3-D models are considered. There is hope, however, to speed this up considerably by using iterative techniques (see Vasco *et al.* 1999, 2003), as only the largest singular values and corresponding vectors are required. The implementation of appropriate techniques

for a faster computation of the SVD is essential for the further success of the proposed method.

Both parts of this algorithm are completely independent. The model modification proposed can be used with standard forward modelling to test hypotheses, while the projection can be used with other schemes of model generation, either automatically or through human intervention.

The algorithm has been successfully applied to both synthetic configurations and models obtained from field data. In all cases it was possible to extract valuable information on model significance and resolution.

There are a few critical points to stress, however:

(i) Note that the true model is unknown. We have to be confident, however, that the model obtained from the inversion is quite close to reality. In the modification scheme we assume that the real model is in some respect similar to its smooth image. If for some reason this is not the case, the approach is not useful.

(ii) As regards the projection algorithm, it should be stressed that it is based on an approximation that is only valid in the linear neighbourhood of the original model. There is no simple method to define the linear neighbourhood, except the direct test by forward modelling. In many cases, however, it can be argued from inspection of the resulting model whether it is admissible or not.

(iii) Once the assumption of linearity has been accepted the most critical step is the partitioning of the sensitivity matrix into range and nullspace. The choice of the truncation threshold can prove quite difficult and the results of our analysis sometimes have to be complemented with additional forward modelling. This is a crucial point as different values for the threshold can lead to significantly different projected models, which do not always really maintain the fit to the data. Our method shares this difficulty with most inversion schemes, which have to adopt a trade-off parameter.

Apart from the results presented here, we believe that the method has great potential in planning future experimental setups. If prior knowledge on the approximate character of the target is available, placements of instrumental site and choice of frequency ranges can be evaluated from subsets of a given sensitivity matrix in order to optimize logistical resources. The use of appropriate subsets of the sensitivity matrix can also be used to study the resolving power of the different kinds of data (TE and TM mode, apparent resistivity and phases, geomagnetic transfer functions).

The algorithm presented here may be the starting point for several further developments: for instance, the particular modification scheme used is by no means the only possible one. Indeed, one can think of many different, more general approaches (e.g. level set methods, image processing techniques) and exploring these possibilities is a promising research aim. In addition, methods for the statistical treatment of the results need to be developed. As we obtain a collection of equivalent models from a guided random process, both sets of models have to be characterized in a rigorous manner. As a starting point, it is possible to use a simple counting scheme to obtain a quantitative measure of the probable model geometry. More sophisticated treatments remain a task for the future.

ACKNOWLEDGMENTS

This work was supported by the Spanish Ministry of Science and Technology, Project BTE2003-03046. Financial support for the stay of GM in Aachen was provided by the *Programa Nacional de Becas* FPU. We wish to thank Jaume Pous, whose invaluable comments considerably improved this paper. We also thank Phil Wannamaker and an anonymous reviewer for many critical remarks and suggestions.

REFERENCES

Anderson, E. *et al.*, 1999. *LAPACK Users' Guide*, 3rd edn, SIAM, Philadelphia, Pennsylvania.

de Groot-Hedlin, C. & Constable, S., 1990. Occam's inversion to generate smooth, two-dimensional models for magnetotelluric data, *Geophysics,* **55,** 1613–1624.

Deal, M.M. & Nolet, G., 1996. Nullspace shuttles, *Geophys. J. Int.,* **124,** 372–380.

Farquharson, C.G. & Oldenburg, D.W., 2004. A comparison of automatic techniques for estimating the regularization parameter in non-linear inverse problems, *Geophys. J. Int.*, **156,** 411–425.

Frommer, A. & Maass, P., Fast CG-based methods for Tikhonov-Phillips regularization, *SIAM Journal of Scientific Computing,* **20,** 1831–1850.

Hansen, P.C., 1998. *Rank Defficient and discrete ill-posed Problems. Numerical Aspects of Linear Inversion*, SIAM, Philadelphia, Pennsylvania.

Lanczos, C., 1961. *Linear Differential Operators*, D. Van Nostr&, London, UK.

Mackie, R., Rieven, S. & Rodi, W., 1997. *Users manual and software documentation for two-dimensional inversion of magnetotelluric data*, GSY-USA, Inc., 2261 Market St., Suite 643, San Francisco, CA 94114, User Documentation.

Mehanee, S. & Zhdanov, M.S., 2002. Two-dimensional magnetotelluric inversion of blocky geoelectric structures, *J. geophys. Res.,* **107,** doi:10.1029/2001JB000 191.

Menke, W., 1984. *Geophysical Data Analysis: Discrete Inverse Theory*, Academic Press, New York.

Monteiro Santos, F., Pous, J., Almeida, E., Queralt, P., Marcuello, A., Mati, H. & Mendes Victor, L., 1999. Magnetotelluric survey of the electrical conductivity of the crust across the Ossa Morena Zone and South Portuguese Zone suture, *Tectonophysics,* **201,** 353–367.

Monteiro Santos, F., Mateus, A., Almeida, E., Pous, J. & Mendes Victor, L., 2002. Are some of the deep crustal condcutive features found in SW Iberia caused by graphite?, *Earth planet. Sci. Lett.*, **201,** 353–367.

Mosegaard, K. & Sambridge, M., 2002. Monte carlo analysis of inverse problems, *Inverse Problems,* **18,** 29–54.

Mosegaard, K. & Tarantola, A., 2002. Probabilistic approach to inverse problems, in *International Handbook of Earthquake and Engineering Seismology, Part A*, pp. 237–265, Academic Press, San Diego, California.

Newman, G.A. & Hoversten, G.M., 2000. Solution strategies for two- and three-dimensional electromagnetic inverse problems, *Inverse Problems,* **16,** 1357–1375.

Nocedal, J. & Wright, S.J., 1999. *Numerical Optimization*, Springer, New York.

Pedersen, L. & Rasmussen, T., 1989. Inversion of magnetotelluric data: a non-linear least-squares approach, *Geophys. Prospect.,* **37,** 669–695.

Portniaguine, O., 1999. Image focusing and data compression in the solution of geophysical inverse problems, *PhD thesis,* University of Utah, Utah.

Portniaguine, O. & Zhdanov, M.S., 1999. Focusing geophysical inversion images, *Geophysics,* **64,** 874–887.

Pous, J., Lana, X. & Correig, A., 1985. Generation of earth stratified models compatible with both ellipticity and phase velocity observations of Rayleigh waves, *Pure appl. Geophys.,* **123**.

Pous, J., Muñoz, G., Heise, W., Melgarejo, J.C. & Quesada, C., 2004. Electromagnetic imaging of variscan crustal structures in SW Iberia: the role of interconnected graphite, *Earth planet. Sci. Lett.,* **217,** 435–450.

Rodi, W. & Mackie, R.L., 2001. Nonlinear conjugate gradients algorithm for 2-{D} magnetotelluric inversions, *Geophysics,* **66,** 174–187.

Rowbotham, P.S. & Pratt, R.G., 1997. Improved inversion through use of the null space, *Geophys. Prospect.,* **62,** 869–883.

Schwalenberg, K., 2000. Die Leitfähigkeitstruktur der Zentralen Anden bei 21°S: Zweidimensionale Modellstudien und Untersuchungen zur Auflösbarkeit, *PhD thesis,* Fachbereich Geowissenschaften, Freie Univ. Berlin.

Schwalenberg, K., Rath, V. & Haak, V., 2002. Sensitivity studies applied to a 2-D resistivity model from the central andes, *Geophys. J. Int.,* **150,** 673–686.

Siripunvaraporn, W. & Egbert, G., 2000. An efficient data-subspace inversion for two-dimensional magnetotelluric data, *Geophysics,* **65,** 791–803.

Tarantola, A., 2004. *Inverse Problem Theory. Methods for Model Parameter Estimation*, SIAM, Philadelpha.

Tarantola, A. & Valette, B., 1982a. Generalized nonlinear inverse problems solved using the least-squares criterion, *Reviews of Geophyics and Space Physics,* **20,** 219–232.

Tarantola, A. & Valette, B., 1982b. Inverse problems = quest for information, *Journal of Geophysics,* **50,** 159–170.

Tikhonov, A.N. & Arsenin, V.Y., 1979. *Methods for Solving Ill-Posed Problems*, Nauka, Moscow.

van den Eshof, J. & Sleijpen, G.S.L., 2004. Accurate conjugate gradient methods for shifted systems, *Applied Numerical Mathematics,* **49,** 17–37.

Vasco, D.W., Johnson, L.R. & Marques, O., Global Earth structure: inference and assessment, *Geophys. J. Int.,* **137,** 381–407.

Vasco, D.W., Johnson, L.R. & Marques, O., 2003. Resolution, uncertainty, and whole Earth tomography, *J. geophys. Res.,* **108,** 2022.

Zhdanov, M.S., 2002. *Geophysical inverse theory and regularization problems*, Elsevier, Amsterdam.